

2 **Determination of muon momentum in the
3 MicroBooNE LArTPC using an improved model of
4 multiple Coulomb scattering**

5 R. Acciarri^g C. Adams^{aa} R. An^h J. Anthony^c J. Asaadi^x M. Auger^a L. Bagby^g
6 S. Balasubramanian^{aa} B. Baller^g C. Barnesⁿ G. Barr^q M. Bass^q F. Bay^y M. Bishai^b
7 A. Blake^j T. Boltonⁱ L. Bugel^m L. Camilleri^f D. Caratelli^f B. Carls^g
8 R. Castillo Fernandez^g F. Cavanna^g H. Chen^b E. Church^r D. Cianci^{l,f} E. Cohen^w
9 G. H. Collin^m J. M. Conrad^m M. Convery^u J. I. Crespo-Anadón^f M. Del Tutto^q
10 D. Devitt^j S. Dytman^s B. Eberly^u A. Ereditato^a L. Escudero Sanchez^c J. Esquivel^v
11 B. T. Fleming^{aa} W. Foreman^d A. P. Furmanski^l D. Garcia-Gamez^l G. T. Garvey^k
12 V. Genty^f D. Goeldi^a S. Gollapinniⁱ N. Graf^s E. Gramellini^{aa} H. Greenlee^g
13 R. Grosso^e R. Guenette^q A. Hackenburg^{aa} P. Hamilton^v O. Hen^m J. Hewes^l C. Hill^l
14 J. Ho^d G. Horton-Smithⁱ E.-C. Huang^k C. James^g J. Jan de Vries^c C.-M. Jen^z
15 L. Jiang^s R. A. Johnson^e J. Joshi^b H. Jostlein^g D. Kaleko^f G. Karagiorgi^{l,f}
16 W. Ketchum^g B. Kirby^b M. Kirby^g T. Kobilarcik^g I. Kreslo^a A. Laube^q Y. Li^b
17 A. Lister^j B. R. Littlejohn^h S. Lockwitz^g D. Lorca^a W. C. Louis^k M. Luethi^a
18 B. Lundberg^g X. Luo^{aa} A. Marchionni^g C. Mariani^z J. Marshall^c
19 D. A. Martinez Caicedo^h V. Meddageⁱ T. Miceli^o G. B. Mills^k J. Moon^m M. Mooney^b
20 C. D. Moore^g J. Mousseauⁿ R. Murrells^l D. Naples^s P. Nienaber^t J. Nowak^j
21 O. Palamara^g V. Paolone^s V. Papavassiliou^o S.F. Pate^o Z. Pavlovic^g E. Piasetzky^w
22 D. Porzio^l G. Pulliam^v X. Qian^b J. L. Raaf^g A. Rafiqueⁱ L. Rochester^u
23 C. Rudolf von Rohr^a B. Russell^{aa} D. W. Schmitz^d A. Schukraft^g W. Seligman^f
24 M. H. Shaevitz^f J. Sinclair^a E. L. Snider^g M. Soderberg^v S. Söldner-Rembold^l
25 S. R. Soleti^q P. Spentzouris^g J. Spitzⁿ J. St. John^e T. Strauss^g A. M. Szelc^l N. Tagg^p
26 K. Terao^f M. Thomson^c M. Toups^g Y.-T. Tsai^u S. Tufanli^{aa} T. Usher^u
27 R. G. Van de Water^k B. Viren^b M. Weber^a D. A. Wickremasinghe^s S. Wolbers^g
28 T. Wongjirad^m K. Woodruff^o T. Yang^g L. Yates^m G. P. Zeller^g J. Zennamo^d C. Zhang^b

29 ^aUniversität Bern, Bern CH-3012, Switzerland

30 ^bBrookhaven National Laboratory (BNL), Upton, NY, 11973, USA

31 ^cUniversity of Cambridge, Cambridge CB3 0HE, United Kingdom

32 ^dUniversity of Chicago, Chicago, IL, 60637, USA

33 ^eUniversity of Cincinnati, Cincinnati, OH, 45221, USA

34 ^fColumbia University, New York, NY, 10027, USA

35 ^gFermi National Accelerator Laboratory (FNAL), Batavia, IL 60510, USA

36 ^hIllinois Institute of Technology (IIT), Chicago, IL 60616, USA

37 ⁱ*Kansas State University (KSU), Manhattan, KS, 66506, USA*
38 ^j*Lancaster University, Lancaster LA1 4YW, United Kingdom*
39 ^k*Los Alamos National Laboratory (LANL), Los Alamos, NM, 87545, USA*
40 ^l*The University of Manchester, Manchester M13 9PL, United Kingdom*
41 ^m*Massachusetts Institute of Technology (MIT), Cambridge, MA, 02139, USA*
42 ⁿ*University of Michigan, Ann Arbor, MI, 48109, USA*
43 ^o*New Mexico State University (NMSU), Las Cruces, NM, 88003, USA*
44 ^p*Otterbein University, Westerville, OH, 43081, USA*
45 ^q*University of Oxford, Oxford OX1 3RH, United Kingdom*
46 ^r*Pacific Northwest National Laboratory (PNNL), Richland, WA, 99352, USA*
47 ^s*University of Pittsburgh, Pittsburgh, PA, 15260, USA*
48 ^t*Saint Mary's University of Minnesota, Winona, MN, 55987, USA*
49 ^u*SLAC National Accelerator Laboratory, Menlo Park, CA, 94025, USA*
50 ^v*Syracuse University, Syracuse, NY, 13244, USA*
51 ^w*Tel Aviv University, Tel Aviv, Israel, 69978*
52 ^x*University of Texas, Arlington, TX, 76019, USA*
53 ^y*TUBITAK Space Technologies Research Institute, METU Campus, TR-06800, Ankara, Turkey*
54 ^z*Center for Neutrino Physics, Virginia Tech, Blacksburg, VA, 24061, USA*
55 ^{aa}*Yale University, New Haven, CT, 06520, USA*

56 **ABSTRACT:** We discuss a technique for measuring a charged particle's momentum by means of
57 multiple Coulomb scattering (MCS) in the MicroBooNE liquid argon time projection chamber
58 (LArTPC). This method does not require the full particle ionization track to be contained inside of
59 the detector volume as other track momentum reconstruction methods do (range-based momentum
60 reconstruction and calorimetric momentum reconstruction). We motivate use of this technique,
61 describe a tuning of the underlying phenomenological formula, quantify its performance on fully
62 contained beam-neutrino-induced muon tracks both in simulation and in data, and quantify its
63 performance on exiting muon tracks in simulation. We find agreement between data and simulation
64 for contained tracks, with a small bias in the momentum reconstruction and with resolutions that
65 vary as a function of track length, decreasing from about 10% for the shortest (one meter long)
66 tracks to 5% for longer (several meter) tracks. For simulated exiting muons with at least one meter
67 of track contained, we find a similarly small bias, and a resolution which is less than 15% for muons
68 with momentum below 2 GeV/c though higher at higher momenta.

69	Contents	
70	1 Introduction and motivation	1
71	2 Multiple Coulomb scattering	2
72	2.1 Tuning the Highland formula for argon	4
73	3 MCS implementation using the maximum likelihood method	6
74	3.1 Track segmentation and scattering angle computation	7
75	3.2 Maximum likelihood theory	7
76	3.3 Maximum likelihood implementation	8
77	4 Range-based energy validation from simulation	8
78	5 MCS performance on beam neutrino-induced muons in MicroBooNE data	10
79	5.1 Input sample	10
80	5.2 Event selection	10
81	5.3 Validation of the Highland formula	11
82	5.4 MCS momentum validation	11
83	5.5 Impact of Highland formula tuning	12
84	6 MCS performance on exiting muons in MicroBooNE simulation	15
85	7 Conclusions	16

86 **1 Introduction and motivation**

87 In this paper we summarize the theory of multiple Coulomb scattering (MCS) and describe how the
88 underlying Highland formula is retuned based on Monte Carlo simulation for use in liquid-argon
89 time-projection chambers (LArTPCs). We present a maximum likelihood based algorithm that is
90 used to determine the momentum of particles in a LArTPC. The only way to determine the mo-
91 mentum of a particle that exits the active volume of a LArTPC is through MCS measurements. We
92 demonstrate that this technique works well for a sample of fully contained muons from Booster
93 Neutrino Beam (BNB) ν_μ charged-current (CC) interactions, and determine the resolutions and bi-
94 ases of the measurement. In addition we demonstrate the performance of the method on simulated
95 exiting tracks.

96
97 MicroBooNE (Micro Booster Neutrino Experiment) is an experiment that uses a large LArTPC
98 to investigate the excess of low energy events observed by the MiniBooNE experiment [1] and to
99 study neutrino-argon cross-sections. MicroBooNE is the first detector of the Short-Baseline Neu-
100 trino (SBN) [2] physics program at the Fermi National Accelerator Laboratory (Fermilab), to be

joined by two other LArTPCs: the Short Baseline Near Detector (SBND) and the Imaging Cosmic And Rare Underground Signal (ICARUS) detector [3]. MicroBooNE also performs important research and development in terms of detector technology and event reconstruction techniques for future LArTPC experiments including DUNE (Deep Underground Neutrino Experiment) [4].

105

The MicroBooNE detector [5] consists of a rectangular time-projection chamber (TPC) with dimensions $2.6 \text{ m} \times 2.3 \text{ m} \times 10.4 \text{ m}$ (width \times height \times length) located 470 m downstream from the Booster Neutrino Beam (BNB) target [6]. LArTPCs allow for precise three-dimensional reconstruction of particle interactions. For later reference, the z axis of the detector is horizontal, along the direction of the BNB, while the x direction of the TPC corresponds to the drift coordinate and the y direction is the vertical direction. The mass of active liquid argon contained within the MicroBooNE TPC volume is 89 tons, out of a total mass of 170 tons.

113

A set of 32 photomultiplier tubes (PMTs) and three planes of wires with 3 mm spacing at angles of 0, and ± 60 degrees with respect to the vertical are located in the TPC for event reconstruction as shown in figure 1. The cathode plane operating voltage is -70 kV. A neutrino in the beam interacts with an argon nucleus and the charged outgoing particles traverse the medium, lose energy and leave an ionization trail. The resulting ionization electrons drift in a 273 V/cm electric field to the wire planes constituting the anode. The passage of these electrons through the first two wire planes induces a signal in the wires, and their collection on the third plane also generates a signal. These signals are used to create three distinct two-dimensional views (in terms of wire and time) of the event. Combining these wire signals allow for full three-dimensional reconstruction of the event, with PMT signals providing information about the absolute drift (x) coordinate. The boundaries of the fiducial volume used in this analysis are set back from the six faces of the active volume by distances of between 20 and 37 cm, depending on the face, to reduce the impact of electric-field non-uniformities near the edges of the TPC. This volume corresponds to a mass of 55 tons.

128

The Booster Neutrino Beam (BNB) is composed predominantly of muon neutrinos (ν_μ) with a peak neutrino energy of about 0.7 GeV. Some of these neutrinos undergo charge-current ($\nu_\mu\text{CC}$) interactions in the TPC and produce muons and other particles. For muon tracks that are completely contained in the TPC, we calculate the momentum with a measurement of the length of the particle's track, or with calorimetric measurements which come from wire signal size measurements. Around half of the muons from BNB $\nu_\mu\text{CC}$ interactions in MicroBooNE are not fully contained in the TPC, and therefore using a length-based or calorimetry-based method to determine the momenta for these uncontained tracks is not a possibility; the only way to determine their momenta is through MCS.

138

139 2 Multiple Coulomb scattering

140 Multiple Coulomb scattering occurs when a charged particle traverses medium and undergoes elec-
141 tromagnetic scattering off atomic nuclei. This scattering perturbs the original trajectory of the par-

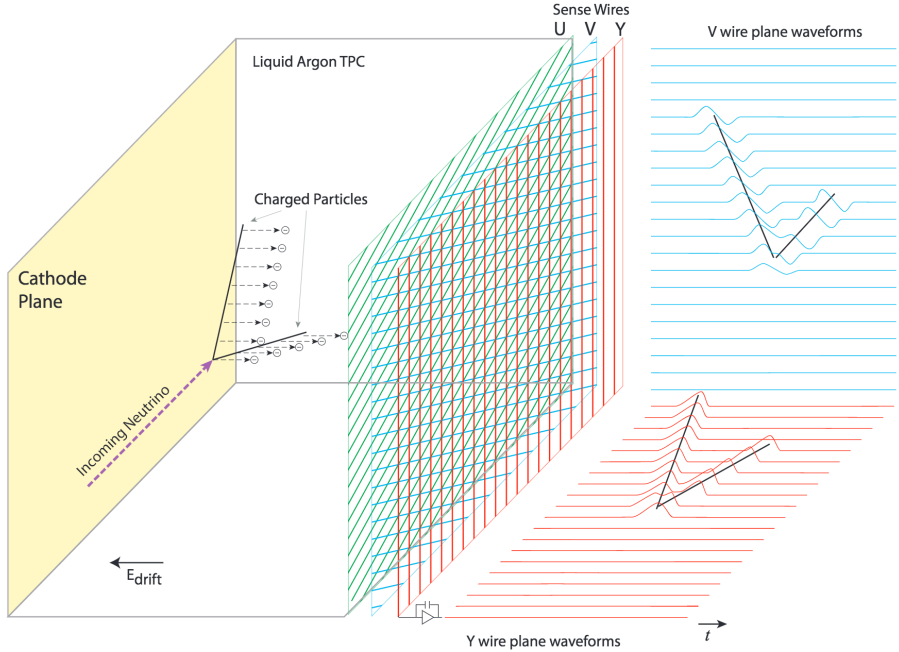


Figure 1. A diagram of the time projection chamber of the MicroBooNE detector [5]. PMTs (not shown) are located behind the wire planes.

ticle within the material (figure 2). For a given initial momentum p , the angular deflection scatters of a particle in either the x' direction or y' direction (as indicated in the aforementioned figure) form a Gaussian distribution centered at zero with an RMS width, σ_o^{HL} , given by the Highland formula [7][8]

$$\sigma_o^{\text{HL}} = \frac{S_2}{p\beta c} z \sqrt{\frac{\ell}{X_0}} \left[1 + \epsilon \times \ln \left(\frac{\ell}{X_0} \right) \right], \quad (2.1)$$

where β is the ratio of the particle's velocity to the speed of light (assuming the particle is a muon), ℓ is the distance traveled inside the material, z is the magnitude of the charge of the particle (unity, for the case of muons), and X_0 is the radiation length of the target material (taken to be a constant 14 cm in liquid argon). S_2 and ϵ are parameters determined to be 13.6 MeV and 0.0038, respectively. In this study, a modified version of the Highland formula is used that includes a detector-inherent angular resolution term, σ_o^{res}

$$\sigma_o = \sqrt{(\sigma_o^{\text{HL}})^2 + (\sigma_o^{\text{res}})^2}. \quad (2.2)$$

For this analysis, the σ_o^{res} term is given a fixed value of 3 mrad which has been determined to be an acceptable value based on simulation studies muons at higher momenta. At 4.5 GeV/c muon momentum and $\ell \approx X_0$, equation 2.1 predicts an RMS angular scatter of 3 mrad, comparable to

155 the detector resolution. The fully contained muons addressed in this analysis have momenta below
156 1.5 GeV/c, making the impact of this detector resolution minimal for that sample.

157

158 With the Highland formula, the momentum of a track-like particle can be determined using
159 only the 3D reconstructed track information, without any calorimetric or track range information.
160 In neutrino physics experiments, emulsion detectors like the DONUT [9] and OPERA [10] Collaborations
161 have used MCS to determine particle momenta. Additionally, the MACRO [11] Collaboration at Gran Sasso Laboratory utilized this technique. The original method for using MCS to determine
162 particle momentum in a LArTPC used a Kalman Filter and was described by the ICARUS
163 collaboration [12], and they more recently described another method [13]. The likelihood-based
164 method, discussed in this paper for use in the Microboone detector and described in detail in section
165 3, has improved on the ICARUS method by tuning the underlying phenomenological formula.
166

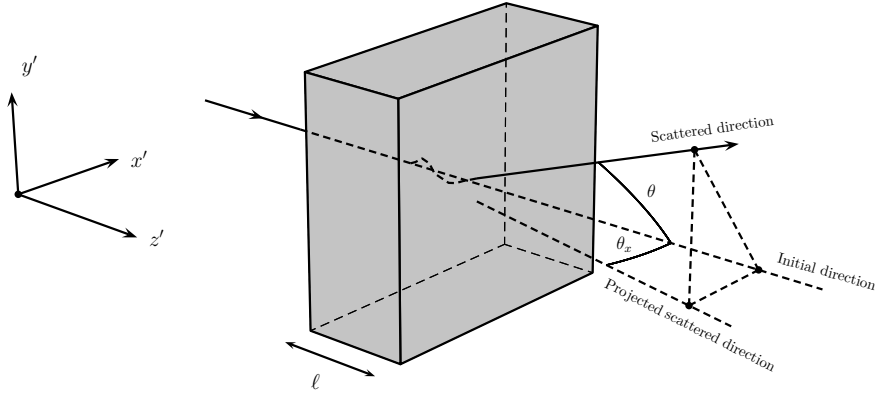


Figure 2. The particle's trajectory is deflected as it traverses the material. The angular scatter in the labeled x' plane is shown as θ_x .

167 2.1 Tuning the Highland formula for argon

168 The Highland formula as written in equation 2.1 originates from a 1991 publication by G. R. Lynch
169 and O. I. Dahl [8]. The parameters in the equation (S_2 and ϵ) were determined using a global fit
170 over MCS simulated data using a modified GEANT simulation package of 14 different elements
171 and 7 thickness ranges. All of the simulated particles were relativistic, with $\beta = 1$. The materials
172 in which they studied scattering ranged from hydrogen (with $Z=1$) to uranium (with $Z=92$). Given
173 that the parameters in the formula were determined from a single fit to a wide range of Z with a
174 wide range of material thicknesses, there is reason to believe that these parameters should differ
175 for scattering specifically in liquid argon with $l \approx X_0$. There is also reason to believe that these
176 parameters might be momentum-dependent for particles with $\beta < 1$, which is the case for some of
177 the contained muons in this analysis.

178

179 In order to re-tune these parameters to liquid argon, a large sample of muons are simulated with
 180 GEANT4 [14] in the MicroBooNE TPC and their true angular scatters are used in a fit, with $l = X_0$.
 181 The reason for using $l = X_0$ is that the Highland formula simplifies to remove its dependence on ϵ

$$\sigma_o^{\text{HL}} = \frac{S_2}{p\beta c}. \quad (2.3)$$

182 The S_2 parameter in equation 2.3 is fit for as a function of true muon momentum at each scatter,
 183 in order to explore the β dependence of this parameter. The fitted parameter value as a function of
 184 true momentum is shown in figure 3.

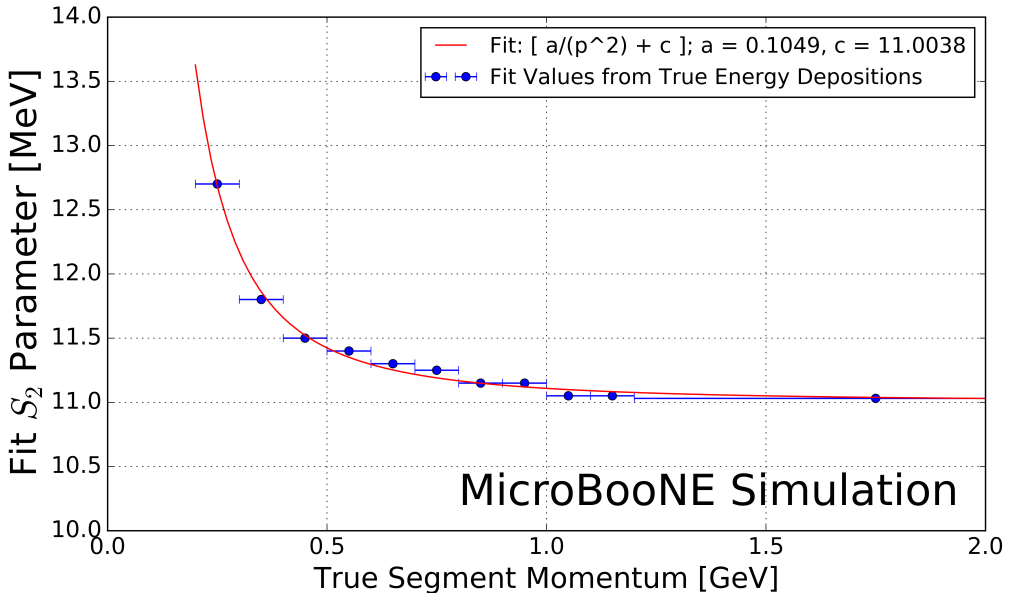


Figure 3. Fitted Highland parameter S_2 as a function of true segment momentum for $\ell = X_0$ simulated muons in the MicroBooNE LArTPC. Blue x- error bars indicate the true momentum bin width with data points drawn at the center of each bin. Shown in red is a fit to these data points with functional form $a \times p^{-2} + c$, with best fit values for parameters a and c shown in the legend.

185 The fitted value of S_2 is always less than the nominal 13.6 MeV for momentum greater than
 186 0.25 GeV/c and asymptotically approaches a constant at higher momentum (where $\beta = 1$) of about
 187 11.0 MeV. The value increases in the momentum region where $\beta < 1$. Shown in red is a fit to
 188 these data points with functional form $a \times p^{-2} + c$, with best fit values for floating parameters a
 189 and c being $0.105 \text{ MeV}^3 c^{-2}$ and 11.004 MeV respectively. This functional form is chosen because
 190 it fits the data well, and asymptotically approaches a constant value when β approaches 1. This
 191 function, used as a replacement for the S_2 parameter in the Highland formula, will henceforth be
 192 referred to as $\kappa(p)$:

$$\kappa(p) = \frac{0.105}{p^2} \text{ MeV}^3 c^{-2} + 11.004 \text{ MeV}. \quad (2.4)$$

193 To visualize the Highland formula for $\ell = X_0$ both before and after the $\kappa(p)$ replacement,
 194 see figure 4. It is recommended that future LArTPC experiments use this parameterization of the

195 Highland formula, or at the very least conduct their own studies to tune the Highland formula for
 196 scattering in argon. This formulation can also be checked in LAr-based test-beam experiments like
 197 LArIAT [15].

198

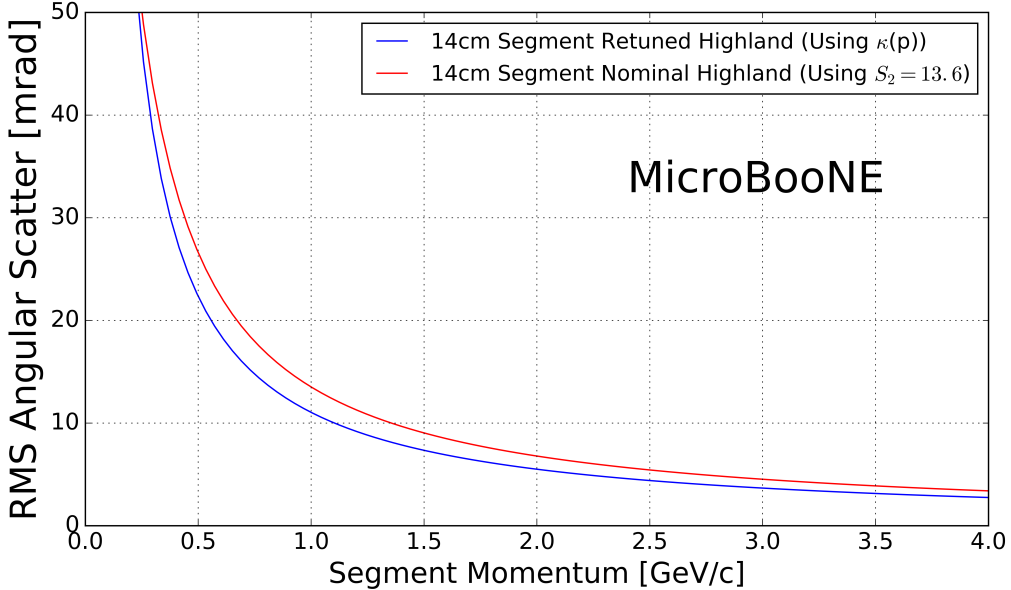


Figure 4. The Highland scattering RMS σ_o^{HL} for 14 cm segment lengths and 0 detector-inherent angular resolution as a function of true momentum before and after tuning. In red is shown equation 2.3 (the nominal Highland formula using $S_2 = 13.6$ MeV) and in blue is the retuned Highland formula (replacing S_2 with $\kappa(p)$).

199

With $\ell = X_0$, the form of the Highland equation used in this analysis is therefore

$$\sigma_o^{\text{RMS}} = \sqrt{(\sigma_o)^2 + (\sigma_o^{\text{res}})^2} = \sqrt{\left(\frac{\kappa(p)}{p\beta c}\right)^2 + (\sigma_o^{\text{res}})^2}. \quad (2.5)$$

200 3 MCS implementation using the maximum likelihood method

201 This section explains in detail how the phenomenon of multiple Coulomb scattering is used to
 202 determine the momentum of a muon track reconstructed in a LArTPC. In general, the approach is
 203 as follows:

- 204 1. The three-dimensional track is divided into segments of configurable length.
- 205 2. The scattering angles between consecutive segments are measured.
- 206 3. Those angles combined with the modified, tuned Highland formula (equation 2.5) are used
 207 to build a likelihood that the particle has a specific momentum, taking into account energy
 208 loss in upstream segments of the track.

209 4. The momentum corresponding to the maximum of the likelihood is chosen to be the MCS-
210 computed momentum.

211 Each of these steps is discussed in detail in the following subsections.

212

213 **3.1 Track segmentation and scattering angle computation**

214 Track segmentation refers to the subdivision of three-dimensional reconstructed trajectory points of
215 a reconstructed track into portions of definite length. In this analysis, the tracks are automatically
216 reconstructed by the “pandoraNuPMA” projection matching algorithm [16]. The algorithm con-
217 structs the three-dimensional trajectory points by combining two-dimensional hits reconstructed
218 from signals on the different wire planes along with timing information from the photomultiplier
219 tubes. The segmentation process begins at the start of the track, and iterates through the trajectory
220 points in order, defining segment start and stop points based on the straight-line distance between
221 them. There is no overlap between segments. Given the subset of the three-dimensional trajectory
222 points that corresponds to one segment of the track, a three-dimensional linear fit is applied to the
223 data points, weighting all trajectory points equally in the fit. In this analysis, a segment length of
224 14 cm is used, which is a tunable parameter that has been chosen as described in the derivation of
225 $\kappa(p)$ (equation 2.4).

226

227 With the segments defined, the scattering angles between the linear fits from adjacent segments
228 are computed. A coordinate transformation is performed such that the z' direction is oriented along
229 the direction of the linear fit to the first of the segment pair. The x' and y' coordinates are chosen
230 such that all of x' , y' , and z' are mutually orthogonal and right-handed, as shown in figure 2. The
231 scattering angles with respect to the x' direction and the y' direction are computed as input to the
232 MCS algorithm. Only the scattering angle with respect to the x' direction is drawn in figure 2.

233 **3.2 Maximum likelihood theory**

234 The normal probability distribution for a scattering angle in either the x' or y' direction, $\Delta\theta$, with
235 an expected Gaussian uncertainty σ_o and mean of zero is given by

$$f_X(\Delta\theta) = (2\pi\sigma_o^2)^{-\frac{1}{2}} \exp\left[-\frac{1}{2}\left(\frac{\Delta\theta}{\sigma_o}\right)^2\right]. \quad (3.1)$$

236 Here, σ_o is the RMS angular deflection computed by the modified, tuned Highland formula
237 (equation 2.5), which is a function of the momentum and the length of that segment. Since energy
238 is lost between segments along the track, σ_o increases for each angular measurement along the
239 track. We therefore replace σ_o with $\sigma_{o,j}$, where j is an index representative of the segment.

240

241 To obtain the likelihood, we take the product of $f_X(\Delta\theta_j)$ over all n of the $\Delta\theta_j$ segment-to-
242 segment scatters along the track. This product can be written as

$$L(\sigma_{o,1}, \dots, \sigma_{o,n}; \Delta\theta_1, \dots, \Delta\theta_n) = (2\pi)^{-\frac{n}{2}} \times \prod_{j=1}^n (\sigma_{o,j})^{-1} \times \exp\left[-\frac{1}{2} \sum_{j=1}^n \left(\frac{\Delta\theta_j}{\sigma_{o,j}}\right)^2\right]. \quad (3.2)$$

243 Rather than maximizing the likelihood it is more computationally convenient to instead min-
 244 imize the negative log likelihood. Inverting the sign and taking $\ln(L)$ gives an expression that is
 245 related to a χ^2 variable:

$$-l(\mu_o; \sigma_{o,1}, \dots, \sigma_{o,n}; \Delta\theta_1, \dots, \Delta\theta_n) = -\ln(L) = \frac{n}{2} \ln(2\pi) + \sum_{j=1}^n \ln(\sigma_{o,j}) + \frac{1}{2} \sum_{j=1}^n \left(\frac{\Delta\theta_j}{\sigma_{o,j}} \right)^2 \quad (3.3)$$

246 3.3 Maximum likelihood implementation

247 Given a set of angular deflections in the x' and y' directions for each segment as described in
 248 section 3.1 a scan is done over the postulated initial energy, E_t , in steps of 1 MeV up to 7.5 GeV.
 249 The step with the smallest negative log likelihood (equation 3.3) is chosen as the MCS energy.
 250 Equation 3.3 includes a $\sigma_{o,j}$ term that changes for consecutive segments because their associated
 251 energy is decreasing. The energy of the j th segment is related to E_t by

$$E_j = E_t - \Delta E_j, \quad (3.4)$$

252 where ΔE_j is the energy loss upstream of this segment, computed by integrating the muon stopping
 253 power curve given by the Bethe-Bloch equation described by the Particle Data Group (PDG) [18]
 254 along the length of track upstream of this segment. Equation 3.4 introduces a minimum allowable
 255 track energy determined by the length of the track, as E_j must remain positive. This value of
 256 segment energy is converted to a momentum p with the relativistic energy-momentum relation
 257 assuming the muon mass, and is then used to predict the RMS angular scatter for that segment
 258 (σ_o) by way of equation 2.5.

259 4 Range-based energy validation from simulation

260 In order to quantify the performance of the MCS energy estimation method on fully contained
 261 muons in data, an independent determination of energy is needed. Range-based energy, E_{range} is
 262 used here because the true energy E_{true} will not be known in analyzing detector data. The stopping
 263 power of muons in liquid argon is well described by the continuous slowing-down approximation
 264 (CSDA) by the particle data group, and agrees with data at the sub-percent level [17] [19] [20].
 265 By using a linear interpolation between points in the stopping power table of ref. [19], the length
 266 of a track can be used to reconstruct the muon's total energy with good accuracy. A simulated
 267 sample of fully contained BNB neutrino-induced muons longer than one meter is used to quantify
 268 the bias and resolution for the range-based energy estimation technique. The range is defined as the
 269 straight-line distance between the true starting point and true stopping point of a muon, even though
 270 the trajectories are not perfectly straight lines. The bias and resolution are computed in bins of true
 271 total energy of the muons by fitting a Gaussian function to a distribution of the fractional energy
 272 difference $(E_{\text{Range}} - E_{\text{True}})/(E_{\text{True}})$ in each bin. The mean of each Gaussian yields the bias for
 273 that true energy bin, and the width indicates the resolution. Figure 5 shows the bias and resolution for
 274 this method of energy reconstruction increases slightly with true muon energy but remains on the
 275 order of (2-4)%. This result demonstrates that range-based energy (and therefore range-based

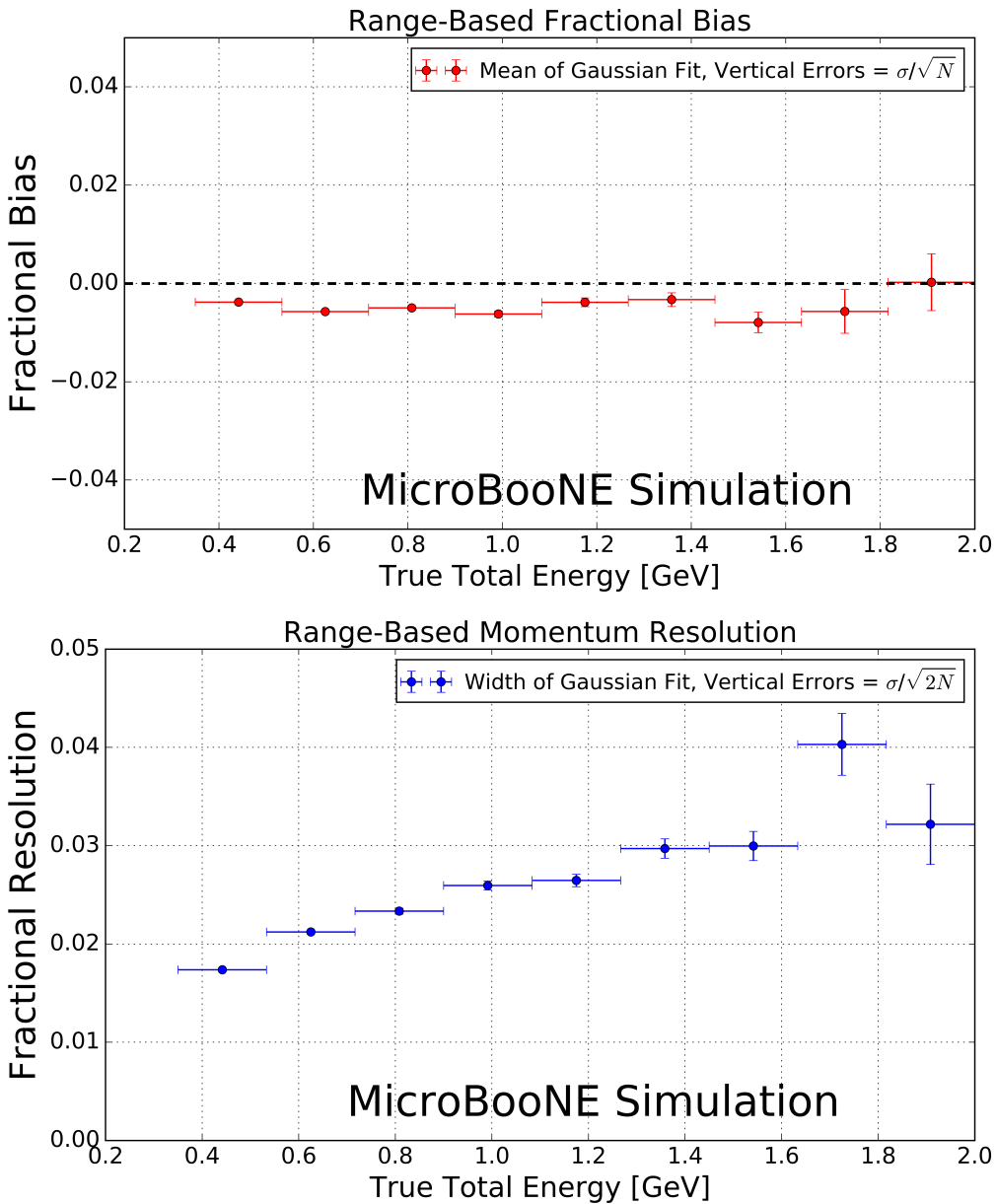


Figure 5. Range-based energy fractional bias (a) and resolution (b) from a sample of simulated fully contained BNB neutrino-induced muons using true starting and stopping positions of the track. The bias is less than 1% and the resolution is below $\approx 4\%$.

277 momentum) is a good estimator of the true energy (momentum) of a reconstructed contained muon
 278 track in data, assuming that the track is well reconstructed in terms of length.

279 **5 MCS performance on beam neutrino-induced muons in MicroBooNE data**

280 **5.1 Input sample**

281 This part of the analysis is based on triggered neutrino interaction events in MicroBooNE corre-
282 sponding to $\approx 5 \times 10^{19}$ protons on target, which is a small subset (<10%) of the nominal protons
283 on target scheduled to be delivered to the detector. These events are run through a fully automated
284 reconstruction chain that produces reconstructed objects including three-dimensional neutrino in-
285 teraction points (vertices), three-dimensional tracks (as described in section 3.1) for each outgoing
286 secondary particle from the interaction, and PMT-reconstructed optical flashes from the interaction
287 scintillation light. The fiducial volume used in this analysis is defined in section 1.

288 **5.2 Event selection**

289 The following selection criteria are placed on the reconstructed objects to select ν_μ charged-current
290 interactions in which a candidate muon track exiting the interaction vertex is fully contained within
291 the fiducial volume:

- 292 1. The event must have at least one bright optical flash, reconstructed from PMT timing signals,
293 in coincidence with the expected BNB-neutrino arrival time.
- 294 2. Two or more reconstructed tracks must originate from the same reconstructed vertex within
295 the fiducial volume.
- 296 3. The z coordinate of the optical flash, as determined by the pulse height and timing of signals
297 in the 32 PMTs, must be within 70 cm of any point on the z projection of the candidate muon
298 track.
- 299 4. For events with exactly two tracks originating from the vertex, additional calorimetric criteria
300 are applied to mitigate backgrounds from cosmic muons that arrive in time with the passage
301 of the beam, then stop and decay to an electron that is reconstructed as a track.
- 302 5. The longest track originating from the vertex is assumed to be a muon, and it must be fully
303 contained within the fiducial volume.
- 304 6. The length of the longest track must be > 1 m in order to have sufficient sampling points in
305 the MCS likelihood to obtain a reasonable estimate of momentum.

306 These selection criteria are chosen to select a sample of tracks with high purity. In this sample
307 of MicroBooNE data, 598 events (tracks) remain after all selections. The low statistics in this
308 sample is due to the size of the input sample, described in section 5.1. Each of these events (tracks)
309 was scanned by hand with a 2D interactive event display showing the raw wire signals of the
310 interaction from each wire plane, with the 2D projection of the reconstructed muon track and vertex
311 overlaid. The scanning was done to ensure the track is well reconstructed with start point close to
312 the reconstructed vertex and end point close to the end of the visible wire-signal track in all three
313 planes. During the scanning, obvious mis-identification topologies were removed. An example of
314 such a topology is a stopping cosmic-ray muon decaying into an electron. After rejecting events
315 (tracks) based on hand scanning, 396 tracks remain for analysis.

316 **5.3 Validation of the Highland formula**

317 The Highland formula indicates that distributions of angular deviations of the track, segment by
 318 segment, in both the x' and y' directions divided by the width predicted from the Highland equation
 319 σ_o^{RMS} (equation 2.5) should be Gaussian with a width of unity. In order to calculate the momentum
 320 p in the Highland equation, p for each segment is computed with equation 3.4, where E_t comes
 321 from the converged MCS-computed momentum of the track. For each consecutive pair of segments
 322 in this sample of 396 tracks, the angular scatter divided by the Highland expected RMS (including
 323 detector resolution term, σ_o^{res}) is an entry in the area-normalized distribution shown in figure 6.
 324 These 396 tracks have on average 12 segments each, therefore this histogram has approximately
 325 $396 \times 12 \times 2 = 9504$ entries. The additional factor of 2 comes from angular scatters both in the x'
 326 and y' directions. The distribution has an RMS of unity, thus validating the MCS technique used
 327 in this analysis.

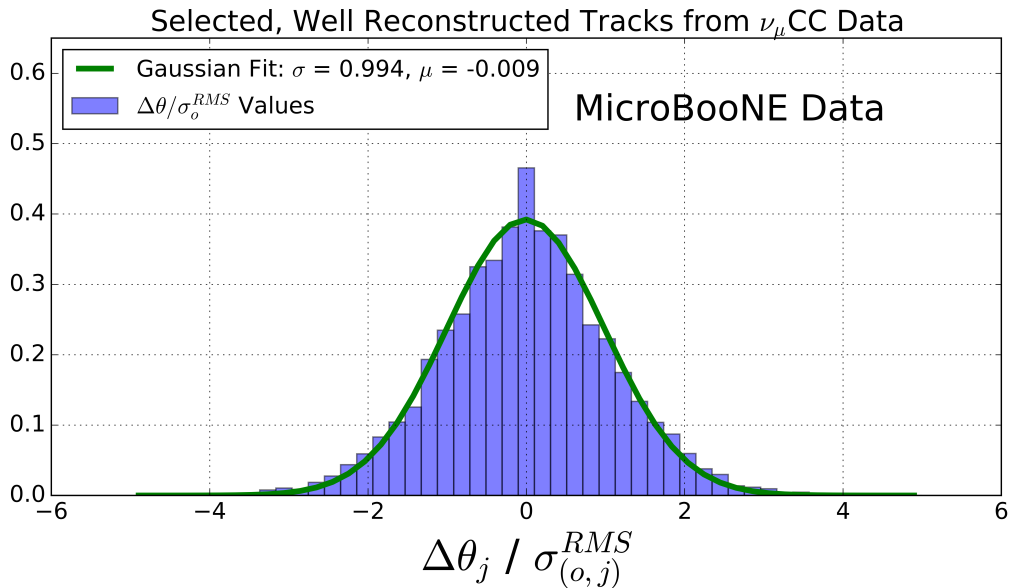


Figure 6. Segment-to-segment measured angular scatters in both the x' and y' directions divided by the width σ_o^{RMS} predicted by the Highland formula (equation 2.1) for the automatically selected beam neutrino-induced fully contained muon sample in MicroBooNE data after hand scanning to remove poorly reconstructed tracks and obvious mis-identification topologies.

328 **5.4 MCS momentum validation**

329 MCS momentum versus range-based momentum for this sample of 396 tracks is shown in figure
 330 7. The fractional bias and resolution as a function of range-based momentum for this sample is
 331 shown in figure 8. In order to compute this bias and resolution, distributions of fractional inverse
 332 momentum difference $(p_{\text{MCS}}^{-1} - p_{\text{Range}}^{-1})/(p_{\text{Range}}^{-1})$ in bins of range-based momentum p_{Range} are fit
 333 to Gaussian functions, where the mean of the fit determines the bias while the width of the fit
 334 determines the resolution for that bin. Inverse momentum is used here because the binned dis-
 335 tributions are more Gaussian since the Highland formula measures inverse momentum in terms

336 of track angles that have reasonably Gaussian errors. Simply using the mean and RMS of the
 337 binned distributions yields similar results. Also shown in this figure are the bias and resolutions
 338 for a simulated sample consisting of a full BNB simulation with CORSIKA-generated [21] cosmic
 339 overlays passed through an identical reconstruction and event selection chain. Rather than hand
 340 scanning this sample, true simulation information is used by requiring the longest reconstructed
 341 track to be matched well to the true starting and stopping point of the ν_μ CC muon. This removes
 342 any mis-identifications or interference from the simulated cosmics.

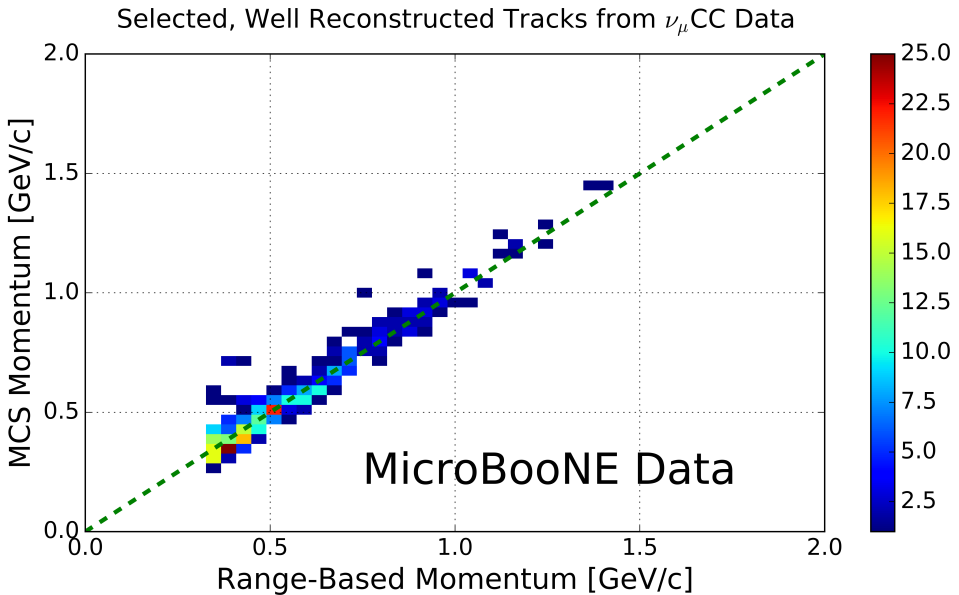


Figure 7. MCS-computed momentum versus range momentum for the automatically selected beam neutrino-induced fully contained muon sample in MicroBooNE data after hand scanning to remove poorly reconstructed tracks and obvious mis-identification topologies. The color (z) scale indicates number of tracks.

343 Figure 8 indicates a bias in the MCS momentum calculation on the order of a few percent, with
 344 a resolution that decreases from about 10% for contained reconstructed tracks in data and simula-
 345 tion with range momentum around 0.45 GeV/c (which corresponds to a length of about 1.5 m) to
 346 below 5% for contained reconstructed tracks in data and simulation with range momentum about
 347 1.15 GeV/c (which corresponds to a length of about 4.6 meters). Resolution improving with length
 348 of track is expected; the longer the track, the more angular scattering measurements can be made
 349 to improve the likelihood. In general the bias and resolutions agree between data and simulation
 350 within uncertainty.

351

352 5.5 Impact of Highland formula tuning

353 In order to examine the impact of the Highland formula tuning described in section 2.1, the frac-
 354 tional bias and resolution on the simulated sample of contained muons described in section 5.4 both
 355 with the nominal Highland formula (equation 2.2) and with the retuned Highland formula (equation

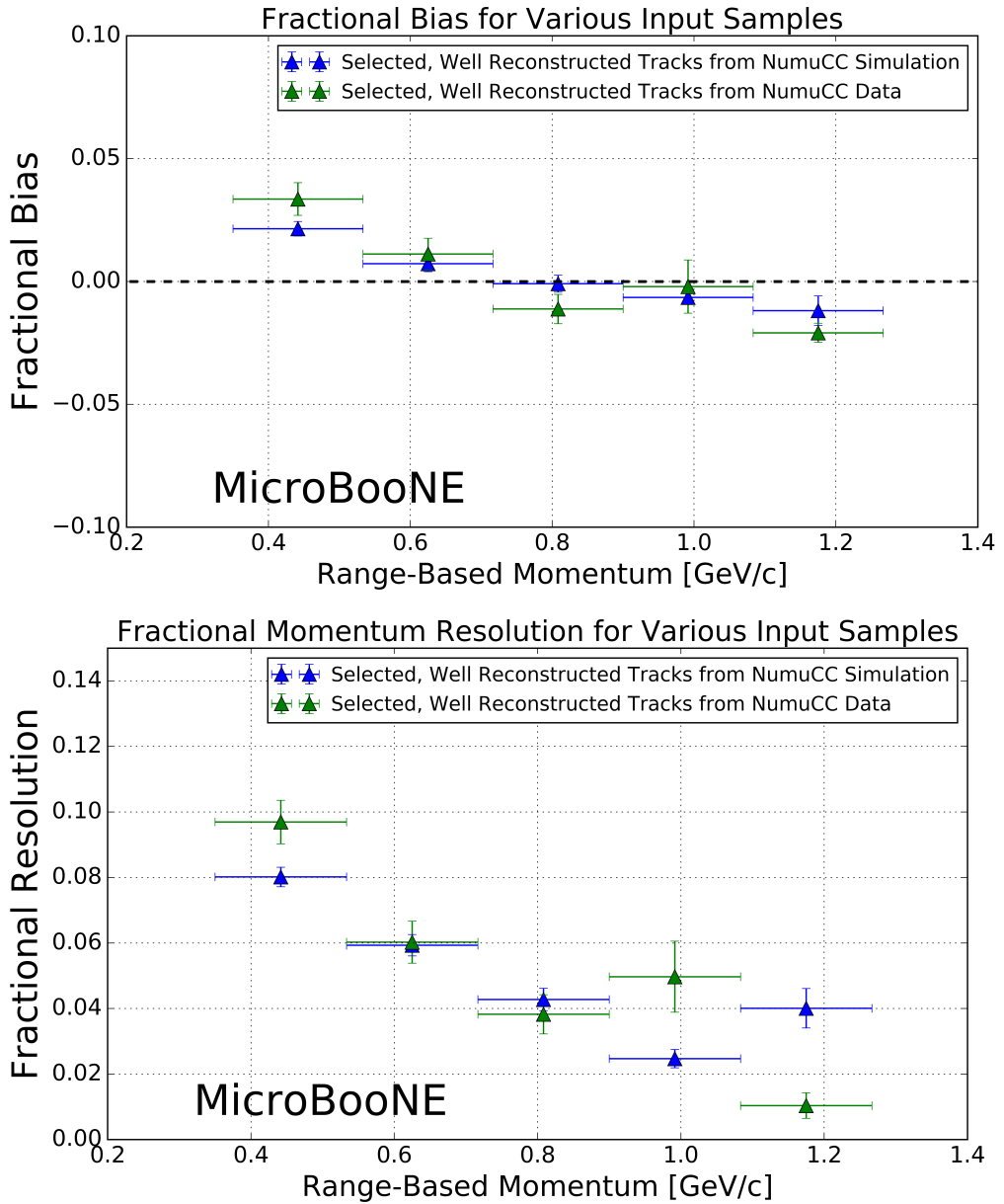


Figure 8. Inverse momentum difference (as defined in the text) fractional bias (top) and resolution (bottom) for automatically selected contained ν_μ CC-induced muons from full simulated BNB events with cosmic overlay where the track matches with the true muon track (blue), and automatically selected (see text) contained ν_μ CC-induced muons from MicroBooNE data (green).

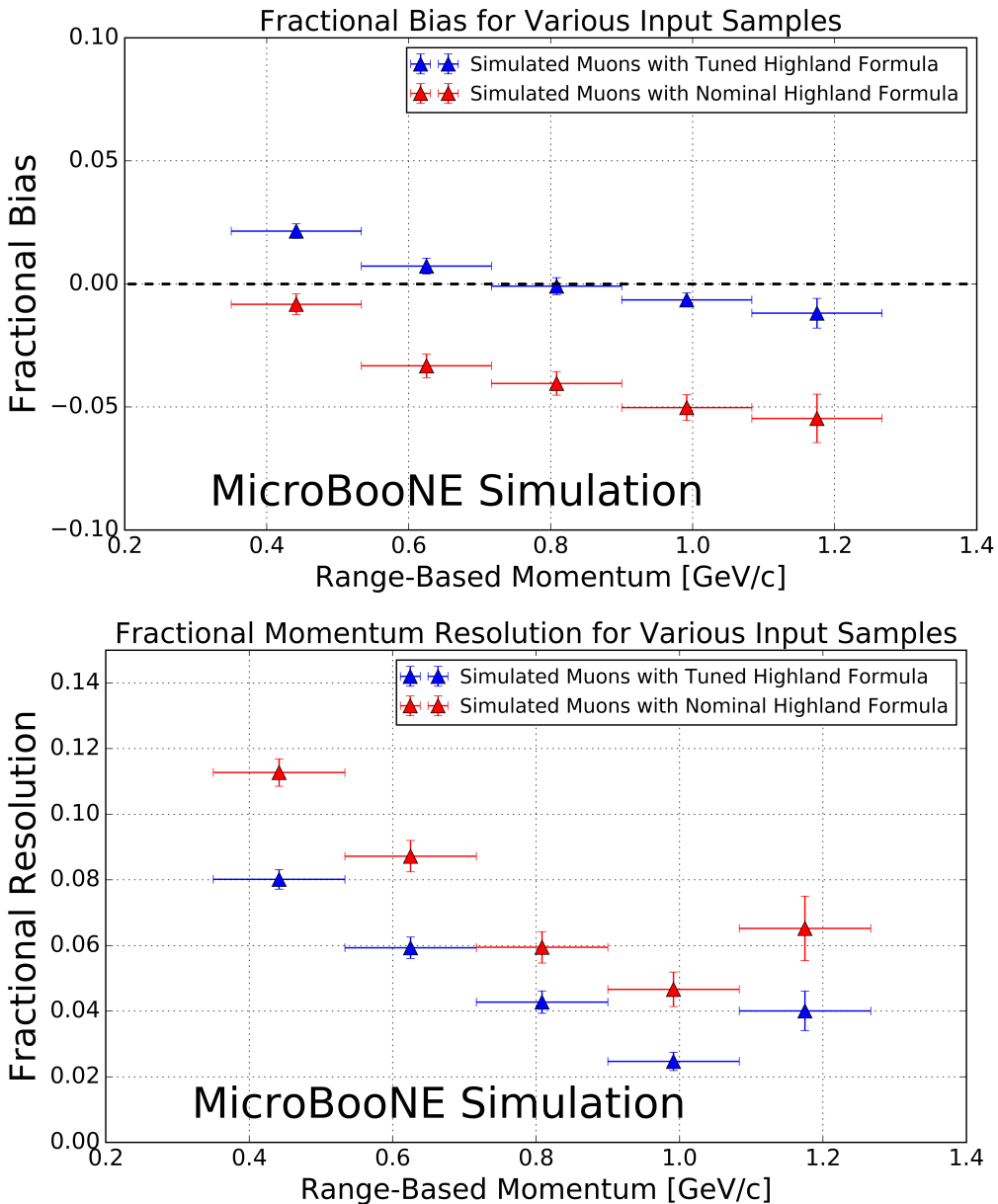


Figure 9. Inverse momentum difference (as defined in the text) fractional bias (top) and resolution (bottom) for automatically selected contained ν_μ CC-induced muons from full simulated BNB events with cosmic overlay where the track matches with the true muon track both using the nominal Highland formula (equation 2.2) (red) and the retuned Highland formula (equation 2.5) (blue).

356 2.5) are shown in figure 9. Tuning the Highland formula improves the magnitude of the fractional
 357 bias to below 2%, and improves the fractional resolution by (2-3)% , with the most improvement at
 358 the lowest momenta.

359 **6 MCS performance on exiting muons in MicroBooNE simulation**

360 In this section we quantify the MCS algorithm performance on a sample of well reconstructed
 361 exiting muon tracks in simulated BNB ν_μ CC interactions within the MicroBooNE detector. The
 362 tracks are automatically reconstructed by the same “pandoraNuPMA” algorithm described in sec-
 363 tion 3.1, and all tracks have a length of at least 1 m within the TPC. This simulation does not include
 364 space-charge effects. The relationship between the MCS and the true momenta at the beginning of
 365 the track as given by simulation for this sample of 28,000 exiting muon tracks is shown in figure 10.
 366

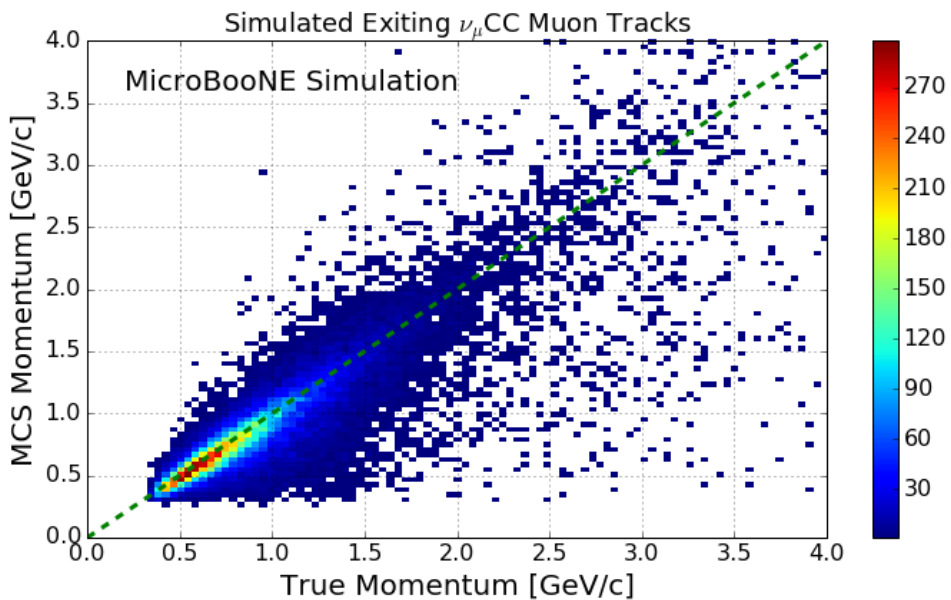


Figure 10. MCS-computed momentum versus true momentum for the sample of simulated exiting BNB ν_μ CC muons in MicroBooNE with at least one meter of track contained within the TPC. The color (z) scale indicates number of tracks.

367 The distribution of $(p_{\text{MCS}}^{-1} - p_{\text{true}}^{-1})/(p_{\text{true}}^{-1})$ is shown for four representative bins of true momen-
 368 tum in figure 11, along with the Gaussian fit to each distribution. Low-momentum tails where the
 369 MCS momentum is underestimated due to poor track reconstruction lie outside the fitted Gaussian
 370 function.

371

372 The fractional bias and resolution as a function of true momentum are shown in figure 12. The
 373 bias is below 4% for all momenta, and the resolution is $\approx 14\%$ in the relevant momentum region for
 374 BNB ν_μ CC muons (below 2 GeV/c). The resolution worsens for muon momenta above this region
 375 because the angular scatters begin to be comparable with the detector resolution term of 3 mrad.
 376 The resolution improves for longer lengths of track contained, with 10% resolution for muons with
 377 $p < 2$ GeV/c with more than 3.5 meters contained. The mean length of track contained for muons
 378 in this analysis is 212 cm.

379

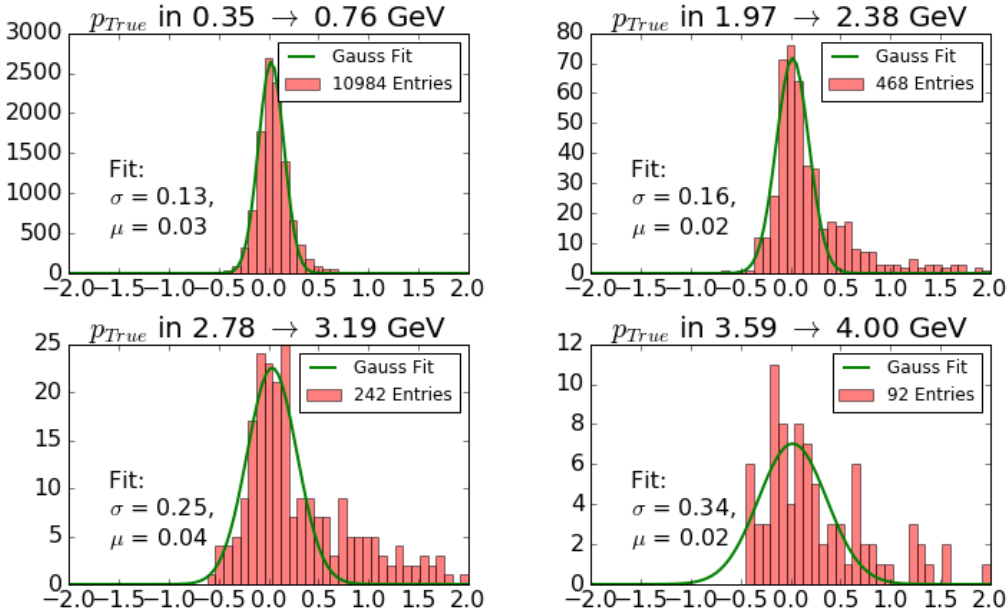


Figure 11. Fractional momentum difference for a few representative bins of true momentum for a sample of simulated exiting muon tracks. The y-axis is number of tracks, and the x-axis is $(p_{\text{MCS}}^{-1} - p_{\text{true}}^{-1})/(p_{\text{true}}^{-1})$.

380 7 Conclusions

381 We have described a multiple Coulomb scattering maximum likelihood method for estimating the
 382 momentum of a three dimensional reconstructed track in a LArTPC and have provided motivation
 383 for development of such a technique. Using simulation, we have shown that the standard Highland
 384 formula should be re-tuned specifically for scattering in liquid argon. After validating range-based
 385 momentum-determination techniques with MicroBooNE simulation, we have demonstrated the ac-
 386 curacy and precision of the MCS-based momentum reconstruction in MicroBooNE data by com-
 387 paring its performance to the range-based method. For 398 fully-contained BNB ν_μ CC-induced
 388 muons, the MCS method exhibits a fractional bias below 3% and a momentum resolution below
 389 10%, agreeing with simulation predictions. Using simulation of a separate sample of uncontained
 390 muon tracks in MicroBooNE with at least one meter contained in the active volume, the MCS-
 391 based reconstruction is shown to produce a fractional bias below 4% and a momentum resolution
 392 of better than 15% for muons in the relevant BNB energy region of below 2 GeV.

393 Acknowledgments

394 This material is based upon work supported by the following: the U.S. Department of Energy,
 395 Office of Science, Offices of High Energy Physics and Nuclear Physics; the U.S. National Science
 396 Foundation; the Swiss National Science Foundation; the Science and Technology Facilities Council
 397 of the United Kingdom; and The Royal Society (United Kingdom). Additional support for the
 398 laser calibration system and cosmic ray tagger was provided by the Albert Einstein Center for
 399 Fundamental Physics. Fermilab is operated by Fermi Research Alliance, LLC under Contract No.
 400 DE-AC02-07CH11359 with the United States Department of Energy.

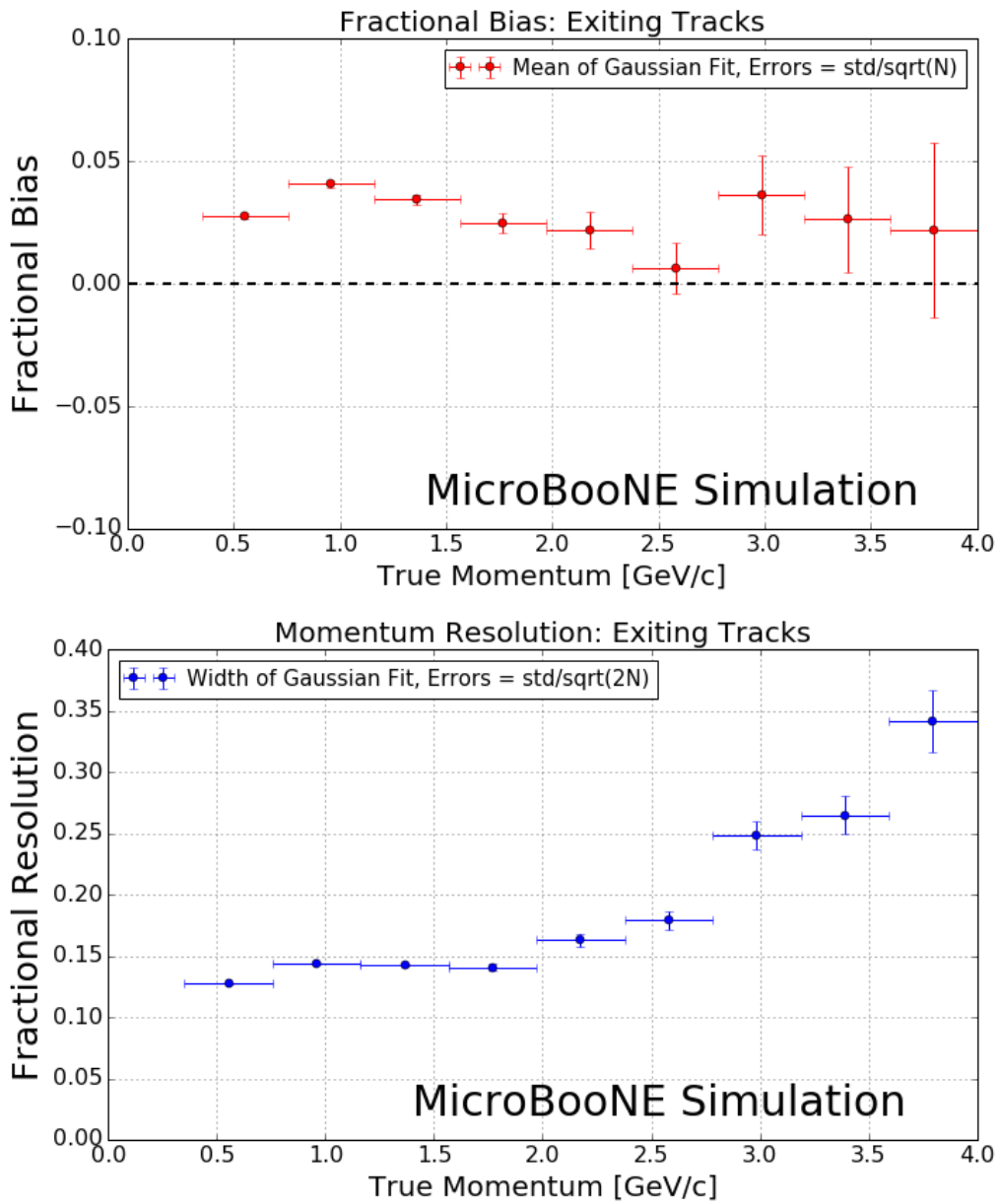


Figure 12. MCS momentum fractional bias (top) and resolution (bottom) as a function of true momentum from a sample of exiting reconstructed muon tracks.

401

References

- [1] A. A. Aguilar-Arevalo *et al.* [MiniBooNE Collaboration], *Improved Search for $\bar{\nu}_\mu \rightarrow \bar{\nu}_e$ Oscillations in the MiniBooNE Experiment*, Phys. Rev. Lett. **110**, 161801 (2013).
[arXiv:1207.4809 [hep-ex], arXiv:1303.2588 [hep-ex]].
- [2] C. Adams *et al.* [LArTPC Collaboration], *LAr1-ND: Testing Neutrino Anomalies with Multiple LArTPC Detectors at Fermilab*, arXiv:1309.7987 [physics.ins-det].
- [3] F. Arneodo *et al.* [ICARUS Collaboration], *The ICARUS experiment: A Second generation proton decay experiment and neutrino observatory at the Gran Sasso Laboratory*, hep-ex/0103008.
- [4] R. Acciarri *et al.* [DUNE Collaboration], *Long-Baseline Neutrino Facility (LBNF) and Deep Underground Neutrino Experiment (DUNE) : Volume 1: The LBNF and DUNE Projects*, arXiv:1601.05471 [physics.ins-det].
- [5] R. Acciarri *et al.* [MicroBooNE Collaboration], *Design and Construction of the MicroBooNE Detector*, arXiv:1612.05824 [physics.ins-det].
- [6] A. A. Aguilar-Arevalo *et al.* [MiniBooNE Collaboration], *The Neutrino Flux prediction at MiniBooNE*, Phys. Rev. D **79**, 072002 (2009)
[arXiv:0806.1449 [hep-ex]].
- [7] V. L. Highland, *Some Practical Remarks on Multiple Scattering*, Nucl. Instrum. Methods **129** (1975) 104-120.
- [8] G. R. Lynch and O. I. Dahl, Nucl. Instrum. Methods Section B (Beam Interactions with Materials and Atoms) **B58**, **6** (1991).
- [9] K. Kodama *et al.* [DONUT Collaboration], *Observation of tau neutrino interactions*, Phys. Lett. B **504**, 218 (2001)
[hep-ex/0012035].
- [10] N. Agafonova *et al.* [OPERA Collaboration], *Momentum measurement by the Multiple Coulomb Scattering method in the OPERA lead emulsion target*, New J. Phys. **14**, 013026 (2012)
[arXiv:1106.6211 [physics.ins-det]].
- [11] G. Giacomelli [MACRO Collaboration], *Neutrino physics and astrophysics with the MACRO experiment at the Gran Sasso lab*, Braz. J. Phys. **33**, 211 (2003)
[hep-ex/0210006].
- [12] A. Ankowski *et al.* [ICARUS Collaboration], *Measurement of through-going particle momentum by means of multiple scattering with the ICARUS T600 TPC*, Eur. Phys. J. C **48**, 667 (2006)
[hep-ex/0606006].
- [13] M. Antonello *et al.*, *Muon momentum measurement in ICARUS-T600 LAr-TPC via multiple scattering in few-GeV range*, arXiv:1612.07715 [physics.ins-det].
- [14] S. Agostinelli *et al.* Nucl. Instrum. Methods Phys. Res. **A506250-303** (2003)
- [15] F. Cavanna *et al.* [LArIAT Collaboration], *LArIAT: Liquid Argon In A Testbeam*, arXiv:1406.5560 [physics.ins-det].
- [16] J. S. Marshall and M. A. Thomson, *The Pandora Software Development Kit for Pattern Recognition*, Eur. Phys. J. C **75**, no. 9, 439 (2015)
[arXiv:1506.05348 [physics.data-an]].
- [17] D. E. Groom, N. V. Mokhov and S. Striganov, *Muon Stopping Power and Range Tables: 10 MeV - 100 TeV Table 5*, <http://pdg.lbl.gov/2012/AtomicNuclearProperties/adndt.pdf>

- 443 [18] H. Bichsel, D. E. Groom, S.R. Klein, *Passage of Particles Through Matter* PDG Chapter 27, Figure
444 27.1 <http://pdg.lbl.gov/2005/reviews/passagerpp.pdf>
- 445 [19] Table 289: Muons in Liquid argon (Ar) [http://pdg.lbl.gov/2012/AtomicNuclearProperties/
446 MUON_ELOSS_TABLES/muonloss_289.pdf](http://pdg.lbl.gov/2012/AtomicNuclearProperties/MUON_ELOSS_TABLES/muonloss_289.pdf)
- 447 [20] *Stopping Powers and Ranges for Protons and Alpha Particles*, ICRU Report No. 49 (1993); Tables
448 and graphs of these data are available at <http://physics.nist.gov/PhysRefData/>
- 449 [21] D. Heck, J. Knapp, J. N. Capdevielle, G. Schatz, T. Throw, *CORSIKA: A Monte Carlo Code to
450 Simulate Extensive Air Showers*, Forschungszentrum Karlsruhe Report FZKA 6019 (1998)